Research in Astron. Astrophys. **2011** Vol. **11** No. **5**, 607–616
http://www.raa-journal.org *http://www.iop.org/journals/raa*

Research in Astronomy and Astrophysics

Possible radio precursors / signatures of the CMEs onset: radio type III bursts and fine structures in the centimeter-metric wavelength region *

Min Wang[1], Guan-Nan Gao[1], Rui-Xiang Xie[1] and Cheng-Ming Tan[2]

[1] National Astronomical Observatories / Yunnan Astronomical Observatory, Chinese Academy of Sciences, Kunming 650011, China; *wm@ynao.ac.cn*
[2] National Astronomical Observatories, Chinese Academy of Sciences, Beijing 100012, China

Received 2010 April 9; accepted 2010 December 9

Abstract Seventy-one occurrences of coronal mass ejections (CMEs) associated with radio bursts, seemingly associated with type III bursts/fine structures (FSs), in the centimeter-metric frequency range during 2003–2005, were obtained with the spectrometers at the National Astronomical Observatories, Chinese Academy of Sciences (NAOC) and the Culgoora radio spectrometer and are presented. The statistical results of 68 out of 71 events associated with the radio type III bursts or FSs during the initiation or early stages of the CMEs indicate that most CMEs contain the emissions of radio type III bursts/FSs near the time of the CME's onset, in spite of their fast or slow speeds. Therefore, we propose that type III bursts and FSs are possible precursors of the onset of CMEs. We stress that the radio type III bursts/FSs in the centimeter-metric wavelength region and the CME transients possibly occurred in conjunction with the origin of the coronal precursor structures. Thus, the statistical results support the suggestions that type III bursts/FSs are indicators of extra energy input into the corona at the CMEs' onset, and that the type III bursts/FSs are produced primarily due to a coronal instability which eventually triggers the CME process. This may signify that the centimeter-metric radio bursts corresponding to or near the CME's onset are caused by the disturbed corona (possibly including minor magnetic reconnections).

Key words: Sun: radio burst — radio fine structure — coronal mass ejection

1 INTRODUCTION

The radio emissions from flares and coronal mass ejections (CMEs) can provide unique diagnostics of energetic electrons from the low corona to 1 AU. In order to study the energy release and particle acceleration and transport, the detection of the onset and development of CMEs, as well as the properties of the magnetic field in flare-CME sources and ambient coronal structures, the associated radio observations are a key tool. In some studies of the determination of the release time, the time of particle release is regarded as energy independent, and researchers found that the inferred injection time of near relativistic electrons (≥ 30 keV) from the Sun's surface in a few cases is consistent with the timing of the type III radio emission (Krucker et al. 1999; Haggerty & Roelof 2002). Over the

* Supported by the National Natural Science Foundation of China.

past three decades, Jackson et al. (1978) suggested that type III bursts are indicators of extra energy being input into the corona at the onset of the CMEs, and type III bursts are produced in conjunction with coronal instability (such as minor magnetic reconnections) that eventually triggers the CME process. In the late 1970's, the white-light ejection transients appeared as large loop or blob-like structures and were observed and investigated. Forty coronal transients have a possible association with meter-wave type III bursts (Jackson et al. 1978). They indicated that the greater numbers of type III bursts occurred some hours before the main portion of the transients, and demonstrated the close relationships between the type III bursts and the coronal transients. Particularly, they indicated the type III bursts possibly occur in conjunction with the origin of the coronal precursor structures. Jackson et al. (1980) pointed out that metric type III bursts are almost always associated with active solar regions. In particular, the occurrence of type III bursts within a few minutes of the onset of the solar flares is well known. Furthermore, those type III bursts whose positions were measured with the Culgoora heliograph generally emanated from the vicinity of the eventual CMEs. They also pointed out that most of the type III bursts of individual events occur near the time of initial motion of the outermost material of the CMEs, i.e., the onset of motion of the transient precursors. Jackson & Hildner (1978) also noted that they had not yet seen a precursor without an accompanying transient, and indicated the presence of a disturbed corona far ahead of the denser portion of the event.

An advantage of detection at radio wavelengths is that for an occulting disk, the nascent stages of a CME may be observed at short radio wavelengths. The radio images can provide signatures of CME liftoff and angular spread in the corona (e.g., Pohjolainen et al. 2001). We have also obtained some radio type III bursts and fine structures (FSs), which included reverse slope type III, type U/V bursts, spikes, zebra patterns and fiber bursts (Yan et al. 2007; Huang et al. 2008), associated with CMEs in the nascent or early stage of a CME during 2003 to 2005. However, it is still under discussion regarding what is the precursor of the CME at the early onset stage: whether the radio type III bursts/FSs result from the closing stage of onset of the CMEs. Moreover, whether the CMEs must produce the radio type III or FSs in the region of centimeter-metric wavelengths is still an open question. Thus, more observational information about the detailed radio emissions (including type III and various FSs) in multi-band around the onset stage of CMEs is needed.

In this paper, we briefly discuss the relationship between the radio bursts and the CME onsets, and the possible precursors of the CMEs as sources for the energetic electrons responsible for the radio type III bursts and FSs, as well as pointing out the diagnostic potential of radio observations of CMEs. In addition, we would like to inquire into whether or not the type III bursts and FSs are in any way related to the onset of CMEs indicated by coronal transients. The observational data selection and the statistical results are presented in Section 2. The observational characteristics associated with the onsets of CME-related radio emissions and analysis are described in Section 3. The discussion of the possible precursors of the CMEs is given in Section 4.

2 DATA SELECTION AND STATISTICAL RESULT

We select a sample of 71 CME events associated with radio emissions (mainly indicating type III bursts, FS bursts, type II and type IV bursts), which covered a time period from 2003 to 2005, and in the centimeter-metric wavelength region (18–1800 MHz, 1.0–2.0 GHz, 2.6–3.8 GHz, and 5.2–7.6 GHz) (see Table 1). The CME data are obtained from the Solar and Heliospheric Observatory (SOHO)/ Large Angle and Spectrometric Coronagraph (LASCO) Experiment. The radio data are observed with the decimetric and microwave radio spectrometers at the National Astronomical Observatories, Chinese Academy of Sciences (NAOC) (Ji et al. 1997, 2000). It is noticed that the NAOC's spectrometers provide data with high time (10 ms) and spectral resolution (10 MHz), so the radio continuum and FS emissions could be observed. The Culgoora spectrometer covers the frequency range of 18 – 1800 MHz. It can detect the type II, III and IV bursts in the meter and decimeter wavelengths.

Table 1 CME Events Related to Radio Bursts at Centimeter-metric Wavelengths

		CMEs			Radio bursts			
						Types		
No.	Date (yymmdd)	Onset Time (UT)	Angle Width (°)	Speed (km s^{-1})	Start Time (UT)	1.0–7.6 (GHz)	0.018–1.8 (GHz)	Peak Flux@2695MHz (sfu)
1	030121	014734	352/8	414*	022420	c,C8.1	II,III,IV	59
2	030121	054038	349/1	602	054936	c,FS,C4.1/SF	III,spikes	140
3	030123	044841^{o}	41	347*	042400	c,C6.0/1N	II,III,spikes	31@2840M
4	030124	033916^{o}	121	445*	031200	c,s,FS,M1.9/1N	II,III,IV	98
5	030409	225901	257/268	511	232449	c,FS,M2.5/1F	II,III	140
6	030423	004600	271/297	916	005654	s,M5.1/1N	II,III,IV	470
7	030526	054040^{o}	151/148	228*	052226	c,FS,M1.9/1F	II,III,IV	100
8	030527	051620	91/79	725	054046	c,FS,M1.6/1F	II,III	155
9	030527	225637^{o+}	Halo/67	946	225600	s,FS,X1.3/2B	II,III,IV	910
10	030528	002144^{o}	Halo/292	1366	001350	s,FS,X3.6/2B	II,III,IV	1650
11	030529	004603	Halo/260	1237	005020	s,X1.2/2B	II,III,IV	770
12	030531	022024^{o}	Halo/256	1835	021000	c,M9.3/2B	II,III,IV	1400
13	030605	002241^{o}	265/248	1656	235835	s,FS,C5.1/SF	II,III	7@2840M
14	030606	232640	354/9	770	233000	c,FS,M1.0/1F	II,III	110
15	030615	233940^{o}	Halo/84	2053	231935	c,FS,X1.3/8F	II,III,IV	860
16	030617	223853^{o}	Halo/117	1813	222042	c,FS,M6.8	II,III,IV	2100
17	030825	024437^{o}	106/120	575	022727	c,s,FS,C3.6/1F	III	26
18	031021	033040^{o}	Halo/117	1484	032855	s,C7.9/SF	II,III	170
19	031024	023426^{o}	113/113	1055	021421	s,M7.6/1N	III,IV ,FS	560
20	031025	040322^{o}	127/103	685	035617	s,M1.2/2N	II,III,FS	64
21	031026	061340^{o}	108/56	1371	055010	c,FS,X1.2/3B	II,III,IV	34
22	031103	010545^{o}	304/324	827	004844	s,X2.7/2B	II,III,IV	280
23	031118	074655^{o}	144/168	1223	071317	s,FS,M3.2/2N	II,III,IV	1650
24	031120	073722^{o}	Halo/219	669	071810	s,FS,M9.6/2B	II,III,IV	440
25	031120	232729	245/237	494*	234133	c,M5.8/2B	III	745
26	040106	055800	88/88	1469	061305	s,M5.8	III	340
27	040107	034703	78/116	1581	035400	c,FS,M4.5/2N	II,FS	100
28	040109	015715^{o}	135/126	1217	011404	c,FS,M3.2	III	230
29	040109	045007^{o}	71/67	504	044339	s	II,III	6@2840M
30	040120	073116^{o}	186/193	590	072514	c,FS,M6.1/2N	I, III	130
31	040405	052043	111/125	608	053000	c,s,M7.1/1F	II,III	120
32	040411	040005^{o}	203/237	1645	035728	c,FS,C9.6/1F	III,FS	920
33	040616	035032	72/89	603	041556	c,C2.8	II,III	20@2840M
34	040713	234112	253/294	409*	000836	c,M6.7	II,III	375
35	040722	004419^{o}	184/180	492*	001026	c,M9.1/SB	III,FS	330
36	040725	055336^{o}	297/296	299*	053701	c,M7.1/2B	II,III,IV,FS	735
37	040831	044846	272/267	311*	052955	s,M1.4	II	27@2840M
38	040912	003115^{o}	Halo/132	1328	002000	c,FS,M4.8/2N	II,III,IV	2600
39	041021	015429^{o}	82/80	533	003531	s,C7.8/SF	III,FS	42@2840M
40	041029	232737	108/106	424*	234411	s,FS,C3.1		25@2000M
41	041030	060851	Halo/270	422*	060851	c,FS,M4.2/SF	II,III,FS	150
42	041031	050647^{o}	251/250	265*	052007	c,FS,M2.3/SF	II,III,IV,FS	190
43	041103	012357^{+o}	265/272	379*	012321	c,FS,M2.8/1F	II,III,FS	170
44	041103	032453^{o}	91/89	918	031416	c,FS,M1.6/1N	II,III,IV,FS	1300
45	041104	230101^{o}	338/31	1055	225938	c,M5.4	II,III	1500
46	041106	005237^{o}	Halo/23	818	001603	c,FS,M9.3/2N	II,III,IV,FS	1158@2000M
47	041110	020828^{o}	Halo/302	3387	015943	c,FS,X2.5/3B	II,III,IV,FS	710
48	041201	070358^{o}	0/39	834	065235	c,FS,M1.1/SN	III,IV,FS	145
49	041202	235417^{o}	Halo/333	1216	234456	c,FS,M1.5/2F	II,III,IV,FS	520
50	050101	002114	Halo/90	832	002504	c,FS,X1.7	II,III,IV,FS	815
51	050115	060241^{o}	Halo/359	2049	053048	c,FS,M8.6/SF	II,III,IV,FS	110
52	050120	060858	Halo/288	882	061656	c,FS,X7.1/2B	II,III,IV,FS	8700
53	050417	011318	100/99	354*	013642	c,s,C3.3	II	16@2840M
54	050502	222243	105/137	955	224058	c,s	II III	83

Table 1 — *Continued.*

		CMEs			Radio bursts			
						Types		
No.	Date (yymmdd)	Onset Time (UT)	Angle Width (°)	Speed (km s^{-1})	Start Time (UT)	1.0–7.6 (GHz)	0.018–1.8 (GHz)	Peak Flux@2695MHz (sfu)
55	050512	021406^{o}	91/89	279*	010904	c,s,C9.4/2B	III, FS	65
56	050515	213451	334/326	186*	223000	s,M2.6/SF	II,III,FS	65
57	050517	021317	252/246	311*	022954	c,M1.8/1B	II,III,IV	115
58	050601	021332	96/105	453*	023613	c,FS,M1.7/1B	II,III,FS	63
59	050603	015710	126/148	247*	040646	c,FS,M1.3/1B	II,III	170
60	050603	235106^{o}	173/158	273*	234649	s,c,FS,C6.2/SN	II,III,IV,FS	26@2840M
61	050701	042322	78/74	419*	045515	s,C5.3	II,III	51
62	050709	214852^{+}	75/67	373*	214928	c,FS,M2.8/1N	III,IV,FS	1550
63	050713	011725	292/291	327*	022902	c,FS,M1.1/SF	III,FS	270
64	050727	044121^{o}	Halo/84	1787	043414	c,M3.7	II, III	760
65	050728	061240^{o+}	72/70	573	061142	s,C2.8	II,III	28@2840M
66	050728	214549^{o}	81/90	1478	214213	s,M4.8/SF	II,III	60
67	050730	062108^{o}	Halo/60	1968	061601	c,FS,X1.3/2B	II,III,IV,FS	2100
68	050803	043619	104/115	479*	045551	c,FS,M3.4/1N	II,III,FS	120
69	050822	010149^{o}	Halo/220	1194	004138	c,FS,M2.6/1N	II,III,IV,FS	1750
70	050825	041631	115/75	1327	043506	c,M6.4/1N	III	285
71	051201	021942^{o}	265/245	580	021352	c,C2.1/1N	II	71

Notes: II, III and IV represent radio type II, III and IV bursts respectively. FS represents fine structures (including fiber, zebra, spike, fish, etc.), C and S represent complex and simple bursts respectively. The symbol '*' represents the slow CMEs; '+' represents the radio bursts which occurred near the onset of CMEs; 'o' represents radio bursts which occurred before CME onset.

The mainly statistical results are the following: (1) All events are associated with the radio type III bursts/FSs near the CME's onset except for three CME events, i.e., event Nos. 37, 53, and 71 in Table 1. The absence of type III/FSs emission is perhaps due to their intensities being weaker than the sensitivity of the instruments, i.e., the measurable minimum flux density of the instruments, or indeed there were no type III/FSs emissions in these three events. In order to show the intensity of radio bursts, we have listed the values of the peak flux density of the radio bursts at the single frequency (2695, 2840 or 2000 MHz).

(2) The rate of the CME occurrence with radio type III bursts/FSs is not related to the CME speed. Here 47 out of 71 CMEs are fast speed events ($v \geq$500 km s^{-1}). In this paper, we have dealt with a criterion of the fast CME velocity. We select the velocity values $\geq$ 500 km s^{-1} as the fast CMEs based on the following reasons: observations of the outer corona (2.0–30.0 $R_{\odot}$) suggested the existence of two classes of CME events, i.e., impulsive and gradual CME events before leaving the LASCO field of view. The former shows constant velocity which is typically greater than 750 km s^{-1}. The latter displays a persistent and weak acceleration with the velocity in the range 400 to 600 km s^{-1} (Sheeley et al. 1999). Although there is no convincing statistical evidence as yet to suggest the existence of two distinct classes of CME events, the velocity has consistently shown that there is a continuous distribution of velocity from tens to about 2500 km s^{-1} with a single peak at about 300–400 km s^{-1} (Howard et al. 1985). In addition, Kim et al. (2009) indicated the CMEs move outward through the corona at velocities from 10 to $\geq$ 2000 km s^{-1}. They have observed a typical CME event with an average velocity of about 360 km s^{-1} and a velocity of about 470 km s^{-1} at the height of 1.7 $R_{\odot}$. It is obvious that both fast and slow speed CMEs are associated with type III bursts/FSs (e.g., Figs. 1 and 2). Figures 1 and 2 show the time profiles of radio type III bursts/FSs in two events at the selected frequencies corresponding to fast and slow CME events.

(3) The occurrence rate of the fast CMEs each year seems to be decreasing with the descending solar activity cycle (e.g., the rates are about 20/25 (80%) , 16/24 (66%) and 11/22 (50%) from 2003

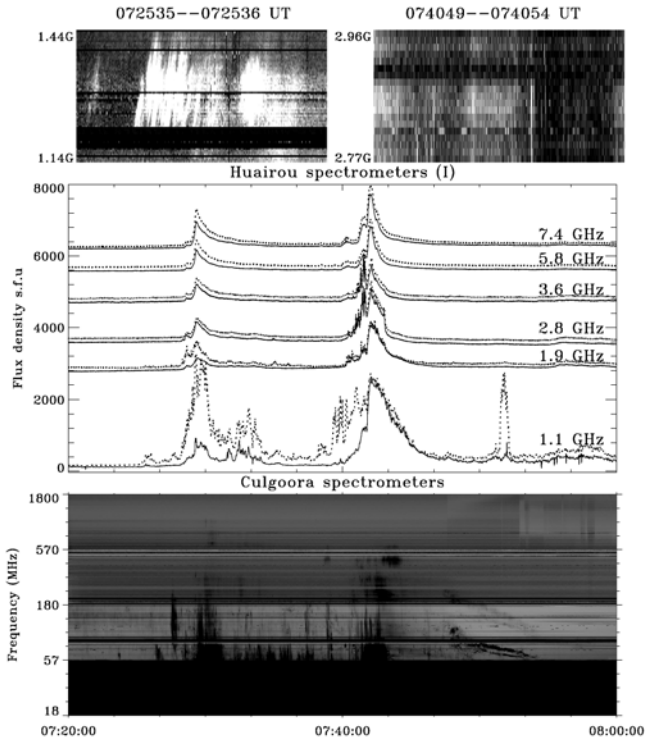

Fig. 1 Event on 2003 Nov. 18. The top panel shows the fine structures. The middle is the time profiles observed with the spectrometers of NAOC, and the solid and dashed lines represent the left circular polarization and right circular polarization, respectively. The bottom is the spectra taken at Culgoora.

to 2005, respectively). Figures panels 3(a), 3(b), and 3(c) show the speed distribution of 71 CME events in 2003, 2004, and 2005, respectively.

(4) In 42 out of 71 events, the radio bursts happened prior to the CMEs' onset. In one event (No. 41 in Table 1), the radio burst occurred simultaneously with the onset, and in 28 events the radio bursts occurred after the onset. In particular, in only 4 events (Nos. 9, 43, 62, and 65 in Table 1) out of 71 events, the radio bursts occurred very near the onset of the CMEs (shortly prior to or after the CME's onset, time interval < 1 min).

3 ANALYSIS

In the present paper, we have selected radio data in the range 18 MHz – 7.6 GHz. At frequencies above 18 MHz, electron acceleration sites are around heights $\leq 2\,R_{\odot}$ (heliocentric distance). So the CME radio precursors are a possible indicator, e.g., the radio type III bursts/FSs caused by the disturbed corona (also including minor magnetic reconnections).

The release time for accelerated particles always coincides with the onset of the complex radio emissions. This suggests that the changes of coronal magnetic processes involved in the radio bursts are related to the origin of the electron acceleration (Maia & Pick 2004). Radio observations in the low corona can contribute to the search for CME precursors. Vourlidas (2004) has reviewed two phenomena: first, the faint drifting continua might indicate the opening of the coronal structures just before the eruption takes place; secondly, the noise storm emission is possibly associated with coronal mass changes. Since the late 1970's, studies have indicated that the radio type III bursts are

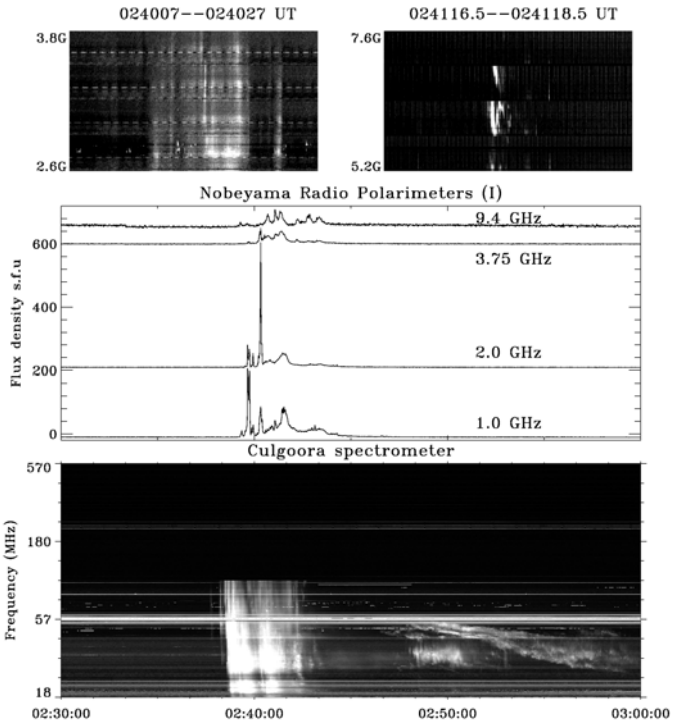

Fig. 2 Event on 2005 June 1. The top panel shows the fine structures. The middle is the time profiles observed with Nobeyama radio polarimeters. The bottom is the spectra of Culgoora.

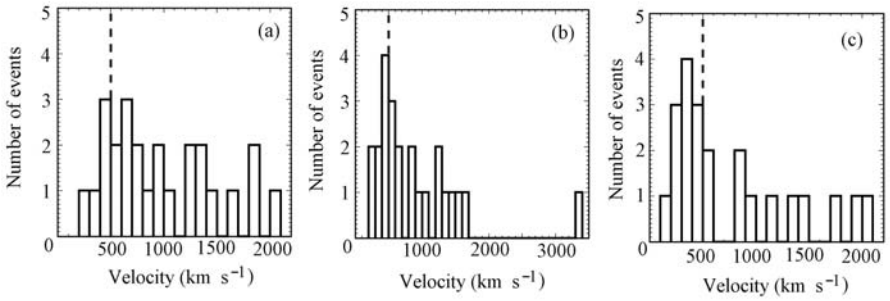

Fig. 3 Histogram of the velocity distribution of CME events, (a) in 2003, (b) in 2004, and (c) in 2005, with 100 km s^{-1} bins.

related to the CMEs' onset through the coronal transients. It was suggested that the type III bursts are an indicator of extra energy input to the corona at the time of CME onset. Another suggestion is that type III bursts are produced in conjunction with a coronal instability which eventually triggers the CME process (Jackson et al. 1978). Jackson & Hildner (1978) indicated that the large magnetic loop or blob-like transient events viewed in the white-light corona are rimmed by the broad region. Above the pre-transient corona region, the density is slightly enhanced. They also indicated that the upper boundaries of the CME precursors develop gradually into the background corona 1 to $\geq 2\,R_{\odot}$ (heliocentric distance) above the transients' leading edges (Jackson & Hildner 1978). It was known

early on that the white light ejection transients appear as large loop or bubble-like structures which carry material outward from the corona (Jackson et al. 1978). As magnetic reconnection sends more and more plasma and magnetic flux into the separatrix bubble, the bubble swells very rapidly. The bubble is often observed by coronagraphs. The magnetic flux contributed by the toroidal magnetic field mainly exists in the flux rope prior to the eruption. The outflow of reconnected plasma and magnetic flux's upward flow is eventually sealed in the separatrix bubble. This creates a rapidly expanding structure, and later leads to the CME lift-off (Lin et al. 2004).

The radio type III bursts/FSs generally start earlier than the main acceleration phase of CMEs. At this time, the signatures of dissipative processes (plasma heating and particle acceleration) are absent in the early stages of the CME, so it is possible that the radio bursts are initially driven by ideal MHD processes (Maričić et al. 2007). The main results from the statistical analysis are as follows:

(1) The possible radio precursors/onset signatures of CMEs as well as their eruption mechanisms occur. Nindos et al. (2008) have mentioned the fact that the type III bursts appeared in the preflare phase (e.g., Benz et al. 1983; Raoult et al. 1985) which indicated the presence of electron acceleration. Such events are often accompanied by the emission of a thermal source in the corona from the footpoints. The observations may imply that the energy supply process that operates in the preflare phase is mostly heating coronal plasma. This process can accelerate particles to nonthermal velocities. Those researchers also reviewed the electron acceleration for the FSs.

In 68 events associated with the type III bursts/FSs, 42 of them occurred prior to the onset of the CMEs, while the others occurred after their onset (see Table 1). This result perhaps implies that the former is the precursor of a CME, and the latter is an early signature of CME development. It is generally agreed that the components of fast time structure indicate that the acceleration of energetic electrons comes from small magnetic structure in the form of nonthermal emissions, while the gradual components of continuum represent energy released from larger magnetic structure in the form of heating (Gopalswamy et al. 1997; Parker 1988). It has also been agreed that particle acceleration sites in solar flares are generally associated with magnetic reconnection regions, or with reconnection-driven shocks. The evidence of magnetic reconnection processes in solar flares has been observed over the last decade (Aschwanden 2002). The observation of initiation and development of the CME by Maričić et al. (2004) indicated that the pre-acceleration phase of the CME concerns the early evolution of the magnetic system. This gradual development is suggestive of an evolution through a series of quasi-equilibrium states. The model (Lin & Forbes 2000) predicts that the precursor should appear before the formation of the neutral X-point in the magnetic field below the flux rope, and before the flare-associated energy release. The possible causes of CME initiation and acceleration have been explored. It has been suggested that a large-scale coronal structure may undergo a stage of quasi-static evolution before reaching an onset of violent magnetic activity. Observations of the energetic solar particles also show that the particles can be trapped, deflected and reaccelerated by the large-scale transient structures (Zhang et al. 2001; Liu et al. 2008). It is possible that the initiation phase of particle acceleration can lead to the eruption of CMEs and flares.

From the above analysis, we think that the occurrence of radio type III bursts/FSs superimposed on the continua at centimeter-metric wavelengths is an important indicator of how a CME evolves. This may support a consideration by Zhang et al. (2001), in which during quasi-static evolution the CME displays a slow ascension, i.e., the so called initiation phase of the CME. Vršnak et al. (2004) also indicated that the gradual evolution can last for several hours prior to the rapid acceleration stage (i.e., main acceleration phase), and indicated that the initial system is evolving through a series of quasi-equilibrium states. Therefore, we may suppose that in this pre-acceleration phase (i.e., the initiation phase, in Zhang et al. 2001) should also appear the precursor of the CME at radio emission from microwave to metric wavelengths, e.g., type III bursts/FSs. Bárta & Karlický (2001, 2005) have developed a model about a variety of FSs which indicated that the decimeter spikes can be generated in the turbulent plasma of reconnection outflows. In these turbulent regions, either decimeter

spikes or other rarer FSs should be observed. Moreover, the radio spikes and type III bursts as tracers of the primary energy release can also be interpreted in terms of ECM (electron cyclotron maser) emission (Fleishman & Mel'Nikov 1998; Aschwanden 2002). The zebra patterns and fiber bursts superimposed on the continua have been observed at decimetric and microwave wavelength ranges (e.g., Altyntsev et al. 2005; Chernov et al. 2003, 2006; Fu et al. 2004). The existing models describing the zebra patterns and fiber bursts have also been summarized (Nindos et al. 2008). Regarding the appearance of zebra patterns, the following are possible explanations: 1) The process is based on the double plasma resonance and subsequent transformation of generated plasma waves into the electromagnetic mode; 2) The process involves the nonlinear coupling of Bernstein modes; 3) The process is based on the eigenmodes of plasma waves trapped in a resonator-like structure formed by local plasma inhomogeneity. Explaining the fiber bursts invokes whistler wave ascending postflare coronal loops, which also act as magnetic traps for nonthermal flare electrons.

(2) Generation mechanism of early development signatures of the CMEs.

The initiation phase of CMEs represents a distinct evolution stage of a CME. It is a CME pre-acceleration phase before the onset of the rapid acceleration. Maričić et al. (2004) found an interesting feature related to the onset of the rapid acceleration: the 'acceleration precursor' occurred roughly simultaneously with the SXR-burst precursor.

Today, two different eruption mechanisms, tether cutting and magnetic breakout, are widely accepted. Sterling & Moore (2004) showed that the tether cutting reconnection may explain the eruption onset when reconnection occurred with only low emission. The tether cutting reconnection was occurring early in the explosive phase and may have further unleashed the explosion; MacNeice et al. (2004) presented the first simulations of the complete breakout process. They indicated that the weaker pre-flare signatures should be present. This is in agreement with their observations, e.g., electron beams were directed from the corona (type III bursts) before the flare's impulsive phase. Sterling & Moore (2004) also suggested a mixed model with slow pre-eruption reconnection at the top of a loop system preceding a fast eruption in the sheared core region.

4 DISCUSSION

Aurass et al. (1999) have shown that the radio spectral data can provide essential information on the timing of the early stage of CME formation and the initial mass motion associated with the ejection. They found that the CME initiation is indicated by a faint group of fast drifting bursts in the meter wavelength, and during the onset of its motion, delayed metric continuum emission is observed. In the present paper, we have observed the short duration radio type III bursts/FSs associated with the CMEs at microwave-metric wavelengths, which mark the initial instability in a small volume before large scale changes. We may suggest that the initial phase of a CMEs is associated with the type III bursts/FSs. This implies that the nonthermal electron beams have nonthermal energy release due to the changes of magnetic topologies in the corona.

The type II radio bursts at microwave-decimetric wavelengths that exhibit close connections with the CMEs and flares (blast waves or flare ejecta acting as a piston) have been established (Maia et al. 2000). A model for the CMEs indicated that their driver is the magnetic free energy stored in a closed, sheared arcade, and their trigger is the reconnection between the sheared arcade and the neighboring flux system occurring in multipolar topologies (Antiochos et al. 1999). Maia et al. (1999) have identified successive sequences in the evolution of the transient coronal activity connected with the CME. Their observational data revealed the initial instability of flares by the occurrence of type III bursts in a small volume at the edge of the flaring region. The radio emission also revealed the existence of expanding loops in the corona. Early in 1982, Kahler found that the metric type II bursts, larger associated flares and accompanying metric type IV bursts are the indicators of CMEs (Kahler 1982). Today, we find that the type III bursts/FSs at centimeter-metric wavelengths most are likely followed by the CMEs. They are possibly the precursors or early signatures of the CME's

onset. In addition, our statistical results seem to be generalizable to all types of CMEs. This aspect remains to be investigated. Whether or not these observational results deserve further investigation and discussion can be argued as follows:

(1) Association of radio type III bursts/FSs with types of CMEs.

A CME has the essential feature that can cause small premature flares to occur. The premature flares can also exhibit large-scale propagating coronal disturbances (Cliver et al. 2005). The small/micro flares possibly correspond to the radio type III bursts/FSs. Most of the CME events listed in Table 1 have radio type III bursts/FSs which occurred before or near the time of the CME's onset. Whatever speed and angular width the CMEs might have, they emit the type III bursts/FSs at microwave or metric wavelengths (e.g., Figs. 1 and 2). This phenomenon mentioned above may be attributed to a common reason, i.e., the initial instability in a small volume of the active region. Whatever multipolar (e.g., Uchida et al. 1999) or single bipolar (e.g., Moore et al. 2001) magnetic systems are involved in the CME development, the transient structures are illuminated by the radio type III burst/FS emissions. Immediately following the type III bursts/FSs, the magnetic systems expand and may unleash even more CMEs (e.g., Maia et al. 1999).

(2) Relationship between the starting time of type III bursts/FSs and the magnetic models of CME generation.

So far, it is rather unclear how the times of pre-/onset-CME radio emissions are related to those initiations of CMEs. Our statistical results also show the complexity of the temporal relationship between the onset of the radio emission and the CMEs. The reason is perhaps caused by the different topological features of magnetic configurations prior to the eruptions. Different magnetic models of CME generation possibly cause the radio flares (bursts) at different times, e.g., there are three widely accepted models about CME/flare eruption: a) the sheared arcade model (Mikic & Linker 1994) that could simultaneously cause flare and disruption of the magnetic field. The preliminary application of the sheared arcade model with helmet streamers indicates that it describes the initiation of CMEs rather well (Mikic & Linker 1994); b) the magnetic breakout model (Antiochos et al. 1999) where the flare erupts first and the CME follows. The most important feature of the magnetic breakout model is the reconnection occurring above the erupting arcade. This reconnection is not expected to release much energy. Although it is unlikely to produce significant energy or strong radio emission, it may emit microwave radio emission from the nonthermal electrons accelerated by this reconnection. The microwave radio observations can provide the best test of this model for CME initiation (Antiochos et al. 1999); c) the catastrophe model (Lin & Forbes 2000) where the CME is very likely to appear before the flare. Thus, the radio type III bursts/FSs occur at a different time than when the CMEs are in progress.

With regard to magnetic morphology, to this day there have been two competing magnetic models which include a multipolar setup or a single bipolar structure (e.g., Sterling & Moore 2004; Moore et al. 2001). Both are able to interpret the non-coincident flare and CME onset times. Our statistical results are consistent with the models. Although radio flares (type III bursts/FSs) and CMEs are both symptoms of the same magnetic "disease," they represent the responses in different parts of the magnetic structure. The radio bursts could be driven by the magnetic activity, shear or reconnection within the magnetic structures (Harrison 1995). In this paper, we have mentioned the origin and trigger mechanisms of CMEs associated with solar radio activity, and have introduced the association between the radio emissions in the centimeter-metric wavelength region and the phenomena of the CME onset stage in the temporal regime. The radio data with spatial resolution are necessary for the identification of the CMEs' onset.

Acknowledgements The authors greatly acknowledge the support provided by the online data of SOHO/LASCO. We would like to thank the research group of NAOC for providing radio data. This work is supported by the National Basic Research Program of the MOST (Grant No. 2011CB811403) and by the CAS-NSFC Key Project (Grant No. 10978006).

References

Altyntsev, A. T., Kuznetsov, A. A., Meshalkina, N. S., Rudenko, G. V., & Yan, Y. 2005, A&A, 431, 1037
Antiochos, S. K., DeVore, C. R., & Klimchuk, J. A. 1999, ApJ, 510, 485
Aschwanden, M. J. 2002, Space Sci. Rev., 101, 1
Aurass, H., Vourlidas, A., Andrews, M. D., et al. 1999, ApJ, 511, 451
Bárta, M., & Karlický, M. 2001, A&A, 379, 1045
Bárta, M., & Karlický, M. 2005, ApJ, 631, 612
Benz, A. O., Barrow, C. H., Dennis, B. R., et al. 1983, Sol. Phys., 83, 267
Chernov, G. P., Sych, R. A., Yan, Y., et al. 2006, Sol. Phys., 237, 397
Chernov, G. P., Yan, Y. H., & Fu, Q. J. 2003, A&A, 406, 1071
Cliver, E. W., Laurenza, M., Storini, M., & Thompson, B. J. 2005, ApJ, 631, 604
Fleishman, G. D., & Mel'Nikov, V. F. 1998, Soviet Physics Uspekhi, 41, 1157
Fu, Q., Yan, Y., Liu, Y., Wang, M., & Wang, S. 2004, ChJAA (Chin. J. Astron. Astrophys.), 4, 176
Gopalswamy, N., Zhang, J., Kundu, M. R., Schmahl, E. J., & Lemen, J. R. 1997, ApJ, 491, L115
Haggerty, D. K., & Roelof, E. C. 2002, ApJ, 579, 841
Harrison, R. A. 1995, A&A, 304, 585
Howard, R. A., Sheeley, N. R., Jr., Michels, D. J., & Koomen, M. J. 1985, J. Geophys. Res., 90, 8173
Huang, J., Yan, Y. H., & Liu, Y. Y. 2008, Sol. Phys., 253, 143
Jackson, B. V., Dulk, G. A., & Sheridan, K. V. 1980, Solar and Interplanetary Dynamics, 91, 379
Jackson, B. V., & Hildner, E. 1978, Sol. Phys., 60, 155
Jackson, B. V., Sheridan, K. V., Dulk, G. A., & McLean, D. J. 1978, Proceedings of the Astronomical Society of Australia, 3, 241
Ji, H., Fu, Q., Lao, D., et al. 1997, Acta Astrophys. Sin., 17, 219
Ji, H., Fu, Q., Liu, Y. Y., et al. 2000, Chin. Astron. Astrophs., 24, 387
Kim, Y., Bong, S., Park, Y., Cho, K., & Moon, Y. 2009, ApJ, 705, 1721
Krucker, S., Larson, D. E., Lin, R. P., & Thompson, B. J. 1999, ApJ, 519, 864
Lin, J., & Forbes, T. G. 2000, J. Geophys. Res., 105, 2375
Lin, J., Raymond, J. C., & van Ballegooijen, A. A. 2004, ApJ, 602, 422
Liu, Y., Luhmann, J. G., Müller-Mellin, R., et al. 2008, ApJ, 689, 563
MacNeice, P., Antiochos, S. K., Phillips, A., et al. 2004, ApJ, 614, 1028
Maia, D., Vourlidas, A., Pick, M., et al. 1999, J. Geophys. Res., 104, 12507
Maia, D., Pick, M., Vourlidas, A., et al., 2000, ApJ, 528, L49
Maia, D. J. F., & Pick, M. 2004, ApJ, 609, 1082
Maričić, D., Vršnak, B., Stanger, A. L., & Veronig, A. 2004, Sol. Phys., 225, 337
Maričić, D., Vršnak, B., Stanger, A. L., Veronig, A. M., Temmer, M., & Roša, D. 2007, Sol. Phys., 241, 99
Mikic, Z., & Linker, J. A. 1994, ApJ, 430, 898
Moore, R. L., Sterling, A. C., Hudson, H. S., & Lemen, J. R. 2001, ApJ, 552, 833
Nindos, A., Aurass, H., Klein, K., & Trottet, G. 2008, Sol. Phys., 253, 3
Parker, E. N. 1988, ApJ, 330, 474
Pohjolainen, S., Maia, D., Pick, M., et al. 2001, ApJ, 556, 421
Raoult, A., Pick, M., Dennis, B. R., & Kane, S. R. 1985, ApJ, 299, 1027
Sheeley, N. R., Walters, J. H., Wang, Y., & Howard, R. A. 1999, J. Geophys. Res., 104, 24739
Sterling, A. C., & Moore, R. L. 2004, ApJ, 602, 1024
Uchida, Y., Hirose, S., Cable, S., et al. 1999, PASJ, 51, 553
Vourlidas, A. 2004, DE Gary & CU Keller (Dordrecht: Kluwer), 223
Vršnak, B., Maričić, D., Stanger, A. L., & Veronig, A. 2004, Sol. Phys., 225, 355
Yan, Y., Huang, J., Chen, B., & Sakurai, T. 2007, PASJ, 59, 815
Zhang, J., Dere, K. P., Howard, R. A., Kundu, M. R., & White, S. M. 2001, ApJ, 559, 452